

# Study of the Structure Formation during Compression for Selecting Multiaxial Deformation Conditions for an Mg–Ca Alloy

N. Yu. Yurchenko<sup>a, \*</sup>, N. D. Stepanov<sup>a</sup>, G. A. Salishchev<sup>a</sup>, N. S. Martynenko<sup>b, c</sup>,  
E. A. Luk'yanova<sup>b, c</sup>, L. L. Rokhlin<sup>b</sup>, and S. V. Dobatkin<sup>b, c, \*\*</sup>

<sup>a</sup>Belgorod State University, Belgorod, 308015 Russia

<sup>b</sup>Baikov Institute of Metallurgy and Materials Science, Russian Academy of Sciences, Moscow, 119991 Russia

<sup>c</sup>National University of Science and Technology MISiS, Moscow, 119049 Russia

\*e-mail: yurchenko\_nikita@bsu.edu.ru

\*\*e-mail: dobatkin.sergey@gmail.com

Received February 1, 2018

**Abstract**—The structure homogeneity of the Mg–0.8% Ca alloy is shown to increase with temperature during uniaxial compression. Plastic deformation localizes in narrow and wide deformation bands at 250–350°C. A small number of regions with recrystallized grains is observed only after deformation at 400°C. A relatively homogeneous recrystallized structure with an average grain size of about 20 μm forms after uniaxial compression at  $t = 450^\circ\text{C}$ . Multiaxial deformation at decreasing temperature in the range 450–250°C significantly refines the initial structure of the Mg–0.8% Ca alloy to an average grain size of 2.1 μm. This structure leads to a significant hardening, namely, an increase in the yield strength to 193 MPa and the tensile strength to 308 MPa. The relative elongation after multiaxial deformation increases by more than two times.

**Keywords:** magnesium alloy, compression, multiaxial deformation, mechanical properties, grain size, recrystallization

**DOI:** 10.1134/S0036029518110137

## INTRODUCTION

The main advantages of magnesium alloys as structural materials are a low density, a high specific strength, high damping, workability and machinability, good weldability in some cases, and the ability to absorb shock energy and vibrations; these advantages make them very promising for use in various branches of modern technology, where saving in weight of a structure plays a decisive role [1–3]. Magnesium alloys are widely used in aerospace engineering; rocket engineering (control parts, aircraft seat parts, landing gears, rocket bodies, and others); and automotive, electrical, and other fields.

Magnesium is also well biocompatible with the human body and is able to completely dissolve in it. Magnesium alloys due to these peculiarities can be used in medicine, for example, for producing the orthopedic implants, coronary stents, and fasteners [4–10]. Such implants must have a high plasticity, strength, and a moderate rate of biodegradation. Magnesium does not have high mechanical properties and has a very high corrosion rate. The corrosion rate of magnesium alloys can be changed and their mechani-

cal and biological properties can be enhanced by alloying and grain refining.

Calcium is considered as one of the main elements for alloying the magnesium alloys intended for biomedical implants, since it is nontoxic to the human body and can slow down the rate of biodegradation and is an essential element for the normal functioning of a number of vital body systems, in particular, the bone tissue. Calcium can also exhibit anticarcinogenic properties [11]. Studies have shown that Mg–Ca alloys demonstrate good biocompatibility in vitro and in vivo and increased corrosion resistance when they gradually dissolve in the bone tissue [12]. In addition to the enhancement of the biological properties, calcium as an alloying element can also enhance the mechanical properties of pure magnesium.

The strength and plastic properties of magnesium alloys can be improved and the rate of corrosion can be slowed down by decreasing the grain size [13]. Severe plastic deformation (SPD) is the most effective modern technique to form an ultrafine-grained (UFG) structure [14]. A great number of work is devoted to the most common SPD technique, equal channel angular pressing (ECAP) [15–19], and a

much smaller number of works, to multiaxial deformation of magnesium alloys [20–22]. It is widely believed that any metal forming, including uniaxial compression and, of course, multiaxial deformation (multiaxial isothermal forging), causes a considerable structure heterogeneity. However, a comparison of the structure and the properties of pure copper after ECAP and multiaxial deformation [23, 24] showed that multiaxial deformation resulted in even better mechanical properties and good homogeneity than ECAP does.

The aim of this work is to study the structure formation during compression to select the conditions of multiaxial deformation of an Mg–0.8% Ca alloy and to form a structure and properties after multiaxial deformation.

## EXPERIMENTAL

The object of the study was an Mg–0.8% Ca magnesium alloy. The alloy was cast in an electric resistance furnace in a metal crucible. An ingot 40 mm in diameter and 120 mm long was prepared by casting into a steel mold heated to 150–200°C.

Samples 15 × 35 mm in size were cut from a volume cast Mg–0.8% Ca alloy workpiece. The samples were placed in a Nabertherm furnace for homogenization and were water quenched after 6-h holding at 510°C.

Compression tests were carried out according to Russian Standard GOST 8817–82 (Metals. Compression Testing Technique). Cylindrical samples 10 mm in diameter and 14 mm in length were cut from the as-cast and heat treated (homogenized) alloy. Uniaxial compression was performed on an Instron 300LX universal hydraulic static testing machine at 250, 300, 350, 400, and 450°C and a strain rate of 1 mm/min. The tests were conducted to 75% vertical deformation or to fracture.

Cylindrical samples 10 mm in diameter and 14 mm in length were cut from workpieces for structural examination after multiaxial deformation at decreasing temperature, and samples 15 mm in diameter and 35 mm in length, for studying the mechanical properties after deformation.

Uniaxial compression was performed with an Instron 300LX universal hydraulic static testing machine at a strain rate of 1 mm/min for samples 10 × 14 mm in size and at 2 mm/min for samples 15 × 35 mm in size. The temperature of the beginning of deformation was  $t_b = 450^\circ\text{C}$ . The temperature was decreased between passes at a step of 50°C. Nine passes were carried out in total. The temperature of the end of multiaxial deformation was  $t_e = 250^\circ\text{C}$ . A temperature decrease below this temperature increased the probability of sample fracture. A total true strain after one pass was ~2.5 and a total true strain after nine passes was 22.5.

Tensile tests were carried out according to Russian Standard GOST 11701–84 (Tensile Testing Tech-

niques for Thin Sheets and Ribbons). Flat samples with a gage length of 16 mm and a cross-section of 1.5 × 3 mm were subjected to tensile tests. Deformation of the samples was carried out by uniaxial tension using an Instron 5882 universal testing machine at a temperature of 20°C and a strain rate of  $10^{-3} \text{ s}^{-1}$ .

Samples for metallographic examination were prepared in the following several stages:

(i) grinding on sandpapers with decreasing grain sizes using a Struers A/S LaboPol-5 (Denmark) grinding-and-polishing machine;

(ii) final polishing on a Struers MD-Chem disk using an O–PS (SiC) suspension with an average abrasive particle size of ~50 nm;

(iii) chemical etching in a reagent consisting of 100 mL ethanol, 5 g picric acid, 5 mL acetic acid, and 10 mL water.

Metallographic studies of the cast, homogenized, and deformed samples were carried out on an Olympus GX71 optical microscope (OM) using the Image Scope M analysis software package. The average grain size was determined by the random intercept method using the Image Scope software.

X-ray diffraction (XRD) analysis was performed using a Rigaku Ultima IV diffractometer and  $\text{CuK}\alpha$  radiation in the angle range  $20^\circ$ – $80^\circ$ .

Microstructural examination was carried out using FEI Quanta 200 3D and FEI Nova NanoSEM 450 scanning electron microscopes (SEM) equipped with backscatter electron (BSE) detectors, energy dispersive spectrometry (EDS) attachments, and electron backscatter diffraction (EBSD) attachments. The OIM Analysis Database 6.2 software was used to perform EBSD analysis and to analyze EBSD data. Black lines indicate high-angle boundaries ( $\theta > 15^\circ$ ) and white lines indicate small-angle boundaries ( $2^\circ < \theta < 15^\circ$ ) on the orientation maps.

## RESULTS AND DISCUSSION

### *Initial Structure of the Mg–0.8% Ca Alloy*

The Mg–0.8% Ca alloy was investigated in two initial states, cast and homogenized. Figures 1a and 1b show SEM images of the initial cast structure of the Mg–0.8% Ca alloy. The structure in the cast state consists of a magnesium matrix and a second phase, which is dark in the OM image (see Fig. 1a) and is light-colored (Fig. 1b) in the SEM image (BSE). The matrix mainly exhibits grains 65  $\mu\text{m}$  in average size, but there are several coarse grains the size of which reaches 200  $\mu\text{m}$  (Fig. 1a). A continuous network (average thickness of ~1.1  $\mu\text{m}$ ; Fig. 1b) of the second phase is observed along grain boundaries. The second phase in the form of uniformly distributed equiaxed and elongated particles (average size of some particles is ~2.5  $\mu\text{m}$ ; Figs. 1a, 1b) is also in grain bodies. The volume fraction of these particles is 3.2%. XRD anal-

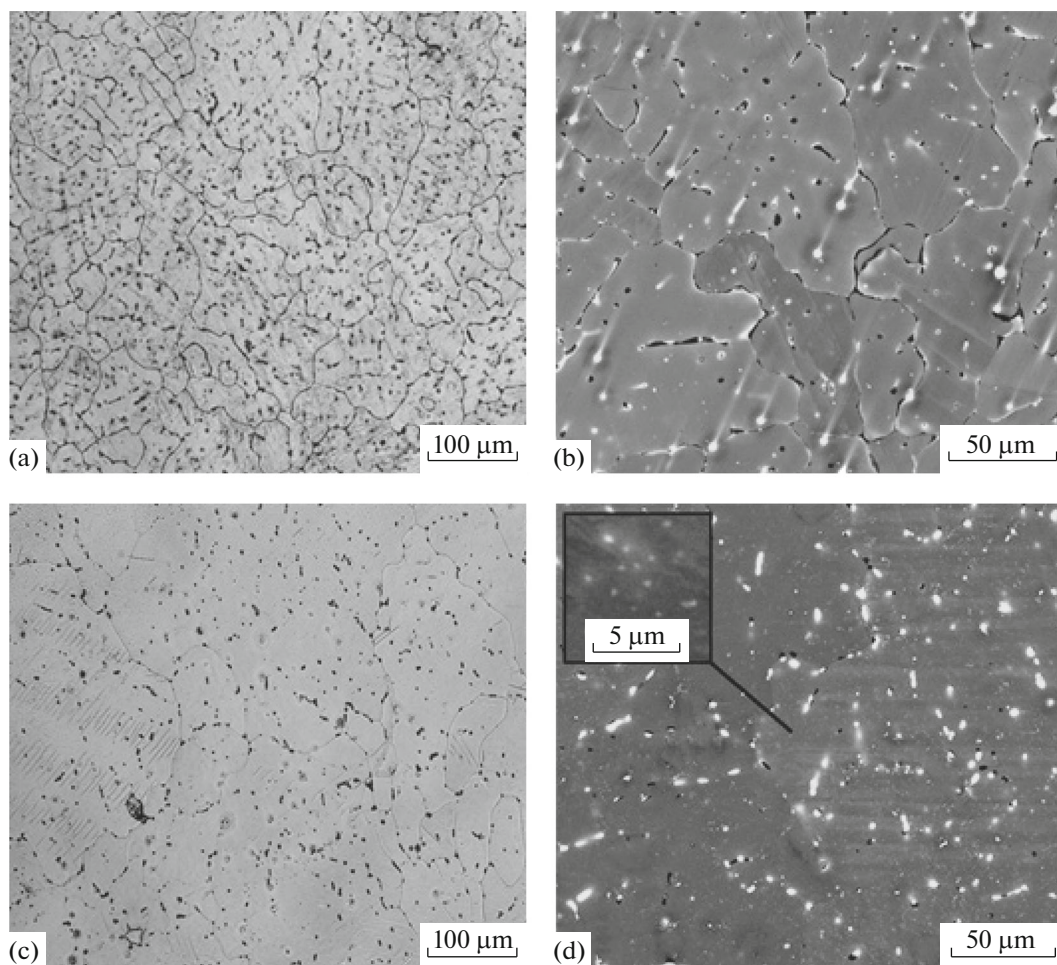


**Fig. 1.** Microstructures ((a, c) OM and (b, d) SEM) of the Mg–0.8% Ca alloy: (a, b) initial as-cast state and (c, d) homogenized state.

ysis suggests that the second phase is represented by  $\text{Mg}_2\text{Ca}$  intermetallic particles. The calcium content in the matrix in the initial as-cast state was  $0.29 \pm 0.03\%$ , according to EDS analysis.

Figures 1c and 1d show the microstructure of the Mg–0.8% Ca alloy after homogenizing annealing. Figure 1c suggests that the average grain size increased to several hundreds of micrometers after homogenizing annealing as compared to that of the as-cast state. Instead of a continuous network of the second phase, both elongated and equiaxed (after coagulation) particles with an average size (transverse) of about  $2.5 \mu\text{m}$  are located along grain boundaries after homogenization (see Figs. 1c, 1d). Their volume fraction is 1.5%. Rather fine (average size of  $\sim 0.3 \mu\text{m}$ ) and uniformly distributed equiaxed particles, the volume fraction of which is  $\sim 1\%$ , should be noted (see Fig. 1d). Some  $\text{Mg}_2\text{Ca}$  intermetallic particles seem to dissolve during homogenization; therefore, the calcium content in the matrix increases to  $0.57 \pm 0.04\%$ .

#### *Mechanical Behavior and Microstructure Evolution in the Mg–0.8%Ca Alloy during Uniaxial Compression*

**As-cast state.** As was mentioned above, uniaxial compression tests were conducted in the temperature range  $250\text{--}450^\circ\text{C}$  to select the conditions of multiaxial deformation of the Mg–0.8% Ca alloy and to study dynamic polygonization and recrystallization processes. Dynamic softening processes are usually studied by structural methods together with investigation of a flow stress–strain ( $\sigma_\varepsilon\text{--}\varepsilon$ ) diagram.

The  $\sigma_\varepsilon\text{--}\varepsilon$  curves of the as-cast Mg–0.8% Ca alloy samples (Fig. 2a) suggest that this dependence upon uniaxial compression is exponential at a deformation temperature  $t = 250^\circ\text{C}$ . However, a linear increase in the flow stress is observed at  $t = 300^\circ\text{C}$ . A steady-state stage of material flow is observed starting from  $350^\circ\text{C}$ . The length of the stage increases when the uniaxial compression temperature is increased. This stage is observed throughout the entire deformation at  $t = 450^\circ\text{C}$ . Table 1 lists data on the dependence between

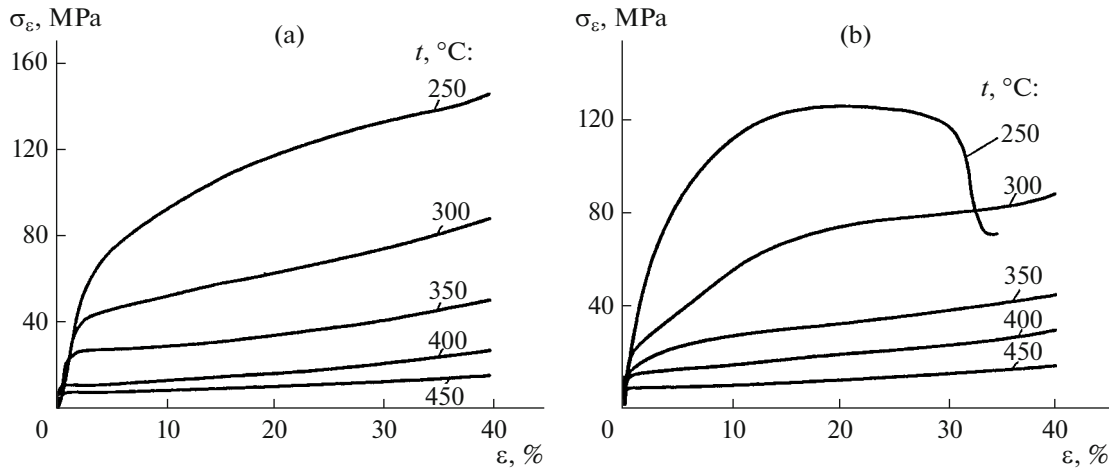


**Fig. 2.** Stress–strain curves for different temperatures of the uniaxial compression of the (a) as-cast and (b) homogenized Mg–0.8% Ca alloy.

yield strength  $\sigma_{0.2}$  and flow stress  $\sigma_{20}$  at a relative strain of 20%. The difference between  $\sigma_{0.2}$  and  $\sigma_{20}$  decreases exponentially when the uniaxial compression temperature is increased.

Figure 3a shows the microstructure of the as-cast Mg–0.8% Ca alloy sample after a 75% uniaxial compression performed at 250°C. The structure is strongly nonuniform and contains a large number of localized deformation zones. There exist individual large areas that are not involved in the process of plastic deformation. At 300°C, the number of the zones at the center of the sample that are not involved in plastic flow decreases. However, there are weakly deformed regions on the periphery of the sample. Uniaxial compression at  $t = 350^\circ\text{C}$  results in a more homogeneous structure (Fig. 3c) as compared to the structure after deformation at 250 and 300°C.

The structure after uniaxial compression of the alloy at  $t = 400^\circ\text{C}$  exhibits a small number of regions with fine recrystallized grains. A heterogeneous recrystallized structure with mainly coarse and irregularly-shaped grains forms during compression at 450°C (Fig. 3e). However, there is a small number of small regular-shaped polyhedral grains located both at the boundaries and in the triple junctions of the coarse grains. The average grain size after compression at  $t = 450^\circ\text{C}$  was about 13  $\mu\text{m}$ .

Figure 4 shows orientational maps of the as-cast Mg–0.8% Ca alloy after uniaxial compression in the range 250–450°C. Figure 4a suggests that localized deformation zones are shear bands. Inside the latter, both regions with a recrystallized structure (average grain size of  $\sim 2 \mu\text{m}$ ) and fragments with low-angle boundaries about 2  $\mu\text{m}$  in size are formed (Fig. 4b). In general, plastic deformation is concentrated mainly only in shear bands, whereas other regions stay out of plastic flow. The propagation of structural homogeneity can be observed after uniaxial compression at  $t =$

450°C (Fig. 4c), which is in agreement with the OM data (see Fig. 3c). At this deformation temperature, the number of undeformed regions is smaller, shear bands expand, and the average size of recrystallized grains in them increases to  $\sim 6 \mu\text{m}$  (see Figs. 4c, 4d).

A relatively homogeneous recrystallized structure with an average grain size of about 20  $\mu\text{m}$  and a fraction of high-angle boundaries of 68.4% forms after uniaxial compression at  $t = 450^\circ\text{C}$  (Fig. 4e).

The size and the volume fraction of  $\text{Mg}_2\text{Ca}$  intermetallic particles in the as-cast Mg–0.8% Ca alloy samples after uniaxial compression were determined by SEM. Fine equiaxed particles should be noted after uniaxial compression of the as-cast Mg–0.8% Ca alloy in the range 250–450°C. For example, Fig. 5a shows average particle size  $D_{\text{pav}}$  and volume fraction  $\phi_p$  of the second phase as functions of the uniaxial compression temperature; i.e., the size of the second phase was calculated using secondary particles, and the fraction of the second phase, using the sum of primary and secondary particles. Two stages can be distinguished in the average particle size–uniaxial compression tem-

**Table 1.** Yield strength  $\sigma_{0.2}$  and flow stress  $\sigma_{20}$  of both as-cast and homogenized Mg–0.8% Ca alloys vs. uniaxial compression temperature  $t$

$t, ^\circ\text{C}$	Mechanical properties of the alloy, MPa			
	cast		homogenized	
	$\sigma_{0.2}$	$\sigma_{20}$	$\sigma_{0.2}$	$\sigma_{20}$
250	35.2	120.0	25.2	127.5
300	28.5	64.8	18.4	75.4
350	20.2	35.7	12.7	35.4
400	10.3	18.1	9.7	21.7
450	7.5	11.4	6.8	11.2

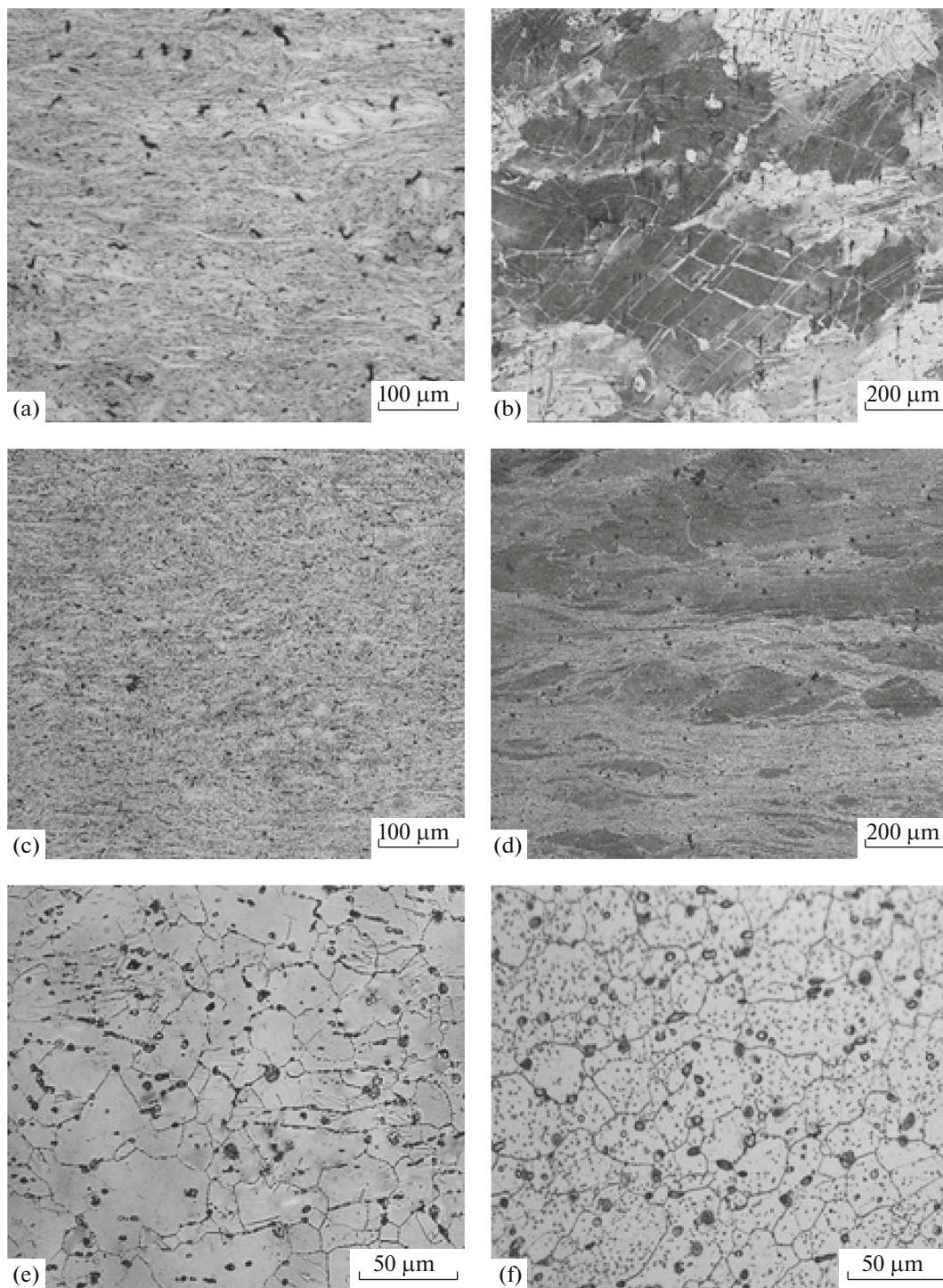


**Fig. 3.** Microstructures (OM) of the Mg–0.8% Ca alloy for (a, c, e) the initial cast state and (b, d, f) homogenized state after 75% uniaxial compression at (a, b) 250, (c, d) 350, and (e) 450°C. A vertical axis coincides with the compression direction.

perature curve. At the first stage (temperature range 250–400°C), the average particle size of  $Mg_2Ca$  increases smoothly and slightly from 0.2  $\mu m$  at 250°C to 0.3  $\mu m$  at 400°C. At the second stage (400–450°C), it increases markedly to  $\sim 0.8 \mu m$ . Two stages can also be distinguished in the curve of the volume fraction of

the second phase versus the uniaxial compression temperature. A noticeable increase in the volume fraction of the second phase is observed at the first stage (temperature range 250–300°C) from 3.6 to 5.3%. However, a further increase in the uniaxial compression temperature to 450°C weakly affects the volume

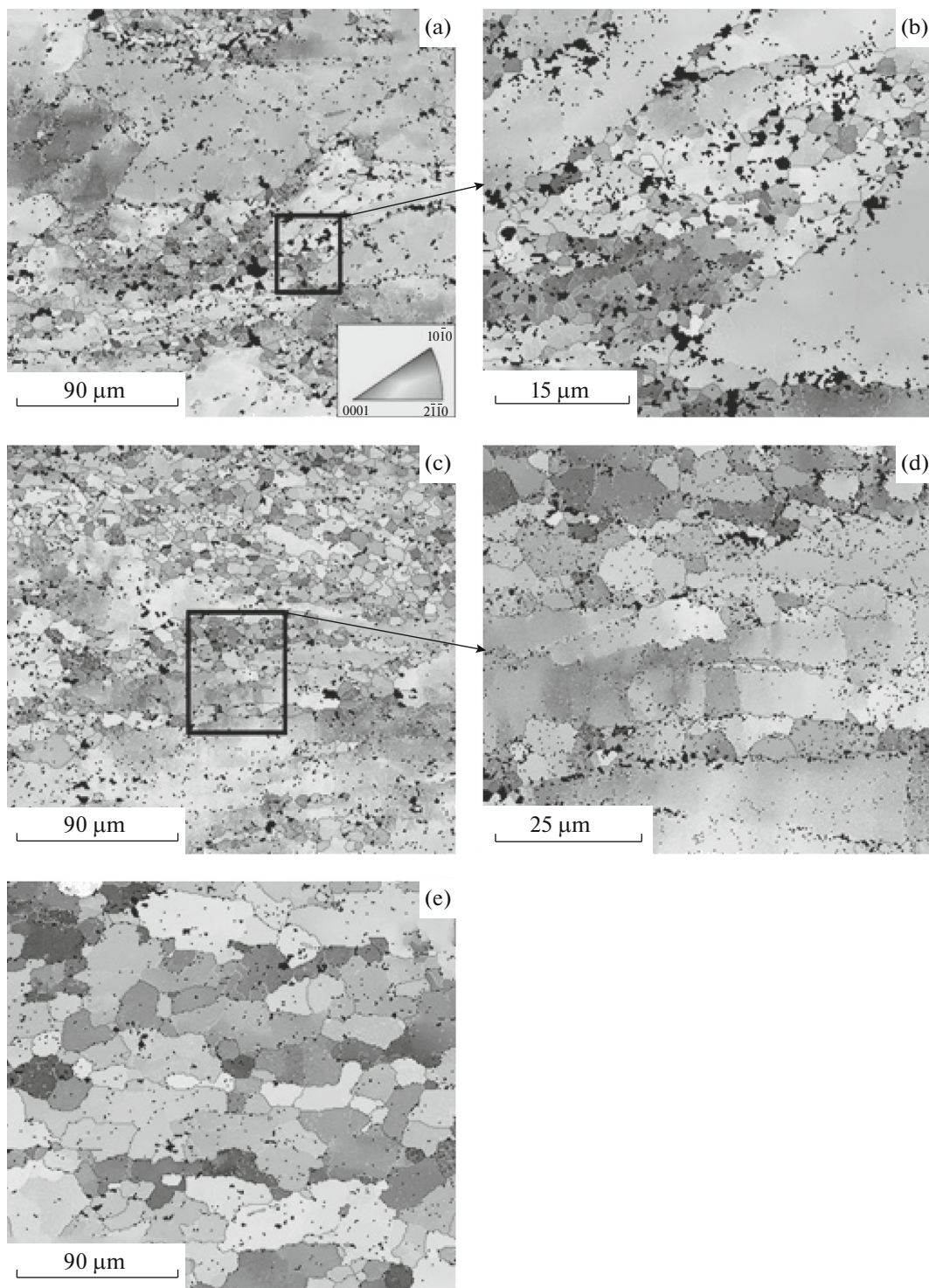


**Fig. 4.** Orientational maps of the Mg–0.8% Ca alloy in the initially cast state after 75% uniaxial compression at (a, b) 250, (c, d) 350, and (e) 450°C.

fraction. The volume fraction of  $Mg_2Ca$  particles at the second stage (300–450°C) is 5.3–5.4%.

**Homogenized state.** Figure 2b depicts the stress–strain ( $\sigma_\epsilon$ – $\epsilon$ ) curves of the homogenized Mg–0.8%

Ca alloy. Uniaxial compression at 250°C results in sharp growth of stresses at vertical strains up to ~15%. The stress varies slightly in the strain range from ~15 to 20% and it decreases at strains above 20%, indicating fracture of the sample. It should be noted that a

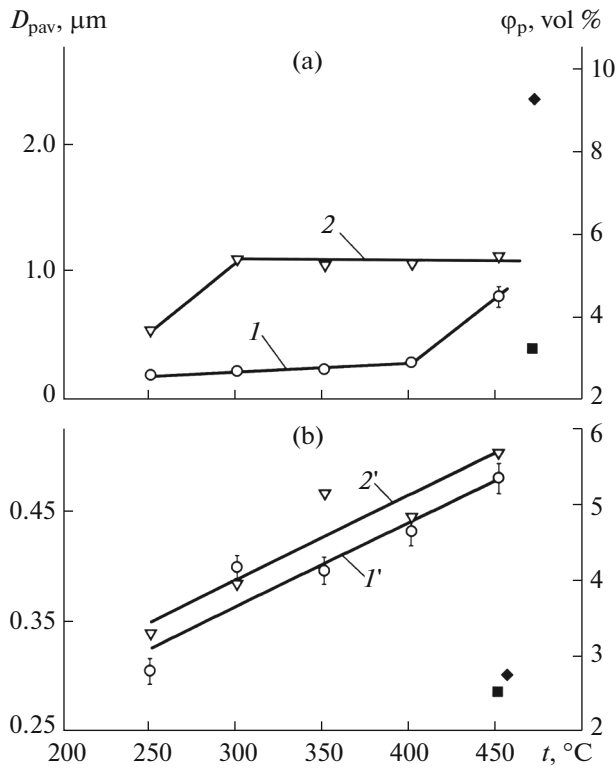


**Fig. 5.** (1, 1') Average size and (2, 2') volume fraction of second-phase particles as functions of the temperature after uniaxial compression of the (a) as-cast and (b) homogenized Mg–0.8% Ca alloy.

homogenized sample upon uniaxial compression at 250 $^{\circ}\text{C}$  failed after a vertical strain of 30% (see Fig. 2b), whereas the as-cast sample at the same temperature was deformed to  $\varepsilon = 75\%$  without fracture. The stress–strain curves of the homogenized and as-cast samples at 300 $^{\circ}\text{C}$  are also different (see Fig. 2b). The following two stages can be identified in the curve: an almost linear dependence of flow stress  $\sigma_e$  on strain  $\varepsilon$  is observed in the region of relative strain to 15%, then a more smooth stress growth during subsequent plastic deformation is observed. Similar stages can be seen in the stress–strain curve at 350 $^{\circ}\text{C}$  (see Fig. 2b). However, in this case, both the length of the first stage (linear stress growth) and the slope of this stage of the curve decrease. No first stage (linear stress growth) at 400 and 450 $^{\circ}\text{C}$ , which was previously noted, is observed. The curves describe only the steady-state flow stage.

Table 1 lists the data characterizing the yield strength–flow stress curve at 20% relative strain of the homogenized Mg–0.8% Ca alloy. It can be seen that the stresses decrease with increasing temperature of uniaxial compression decrease in both the as-cast and homogenized states, and they are almost the same for both cases at 450 $^{\circ}\text{C}$ . It should also be noted that the difference in the values of the yield strength in the as-cast and homogenized states first increases from 28.4% at 250 $^{\circ}\text{C}$  to 37.3% at 350 $^{\circ}\text{C}$  and is within 10%

in the strain range 400–450 $^{\circ}\text{C}$ . In turn, the difference between  $\sigma_{20}$  of both states in the entire temperature range is less than 6%.

Figure 3b shows the structure of the Mg–0.8% Ca alloy sample in the homogenized state after uniaxial compression at 250 $^{\circ}\text{C}$ . Unlike other samples, this sample was deformed only to a strain of  $\sim 30\%$ . Its structure contains a large number of relatively thin, mainly curved, parallel bands. These bands intersect with each other at about a right angle. Uniaxial compression at 250 $^{\circ}\text{C}$  makes grains flat and their boundaries bent (see Fig. 3b). The general picture when the uniaxial compression temperature is increased to 300 $^{\circ}\text{C}$  somewhat changes: narrow localized deformation zones are noted. The shape of both fragments and their boundaries changes greatly as compared to those after compression at 250 $^{\circ}\text{C}$ . The fragments seem to be fragmented into separate regions, whereas their boundaries become more or less continuous. Relatively wide localized deformation zones are observed after uniaxial compression at 350 $^{\circ}\text{C}$ , the fraction of which is about 40–45% (see Fig. 3d). Above 400 $^{\circ}\text{C}$ , regions with recrystallized small grains ( $D_g \approx 8 \mu\text{m}$ ) form. However, a completely recrystallized structure forms only after uniaxial compression at 450 $^{\circ}\text{C}$  (see Fig. 3f). Figure 3f shows that the microstructure is rather homogeneous: clusters of fine regular-shaped polyhedral grains with continuous boundaries are observed together with individual coarse grains. The average grain size after compression at 450 $^{\circ}\text{C}$  was  $\sim 16.5 \mu\text{m}$ .

Figure 6 displays orientational maps of the homogenized Mg–0.8% Ca alloy after uniaxial compression in the temperature range 250–450 $^{\circ}\text{C}$ . Figure 6a suggests that the structure exhibits relatively thin, parallel bands inside coarse initial grains after uniaxial compression at 250 $^{\circ}\text{C}$ , which can also be clearly seen in Fig. 3b. Figure 6b depicts recrystallized grains with an average size of  $\sim 0.8 \mu\text{m}$  inside these bands. It should be specially noted that the misorientation angle between the boundaries of these bands is about 70 $^{\circ}$  with respect to the matrix, and the misorientation of the boundaries inside the coarse initial grains is less than 5 $^{\circ}$ . Figure 6c demonstrates that uniaxial compression at 350 $^{\circ}\text{C}$  divide elongated coarse grains into separate regions by bands, which is in agreement with the OM data (see Fig. 3d). A recrystallized structure with an average grain size of 3  $\mu\text{m}$  is formed inside these bands (Fig. 6d). The regions that form due to the fragmentation of coarse grains by these bands retain their initial orientation. Compression at  $t = 450^{\circ}\text{C}$  results in the formation of a highly nonuniform recrystallized structure with an average grain size of about 20.5  $\mu\text{m}$  and a fraction of high-angle boundaries (HAB) of 75.5% (Fig. 6e).

Figure 5b displays the average particle size and the volume fraction of the second phase as functions of temperature after uniaxial compression of the homog-

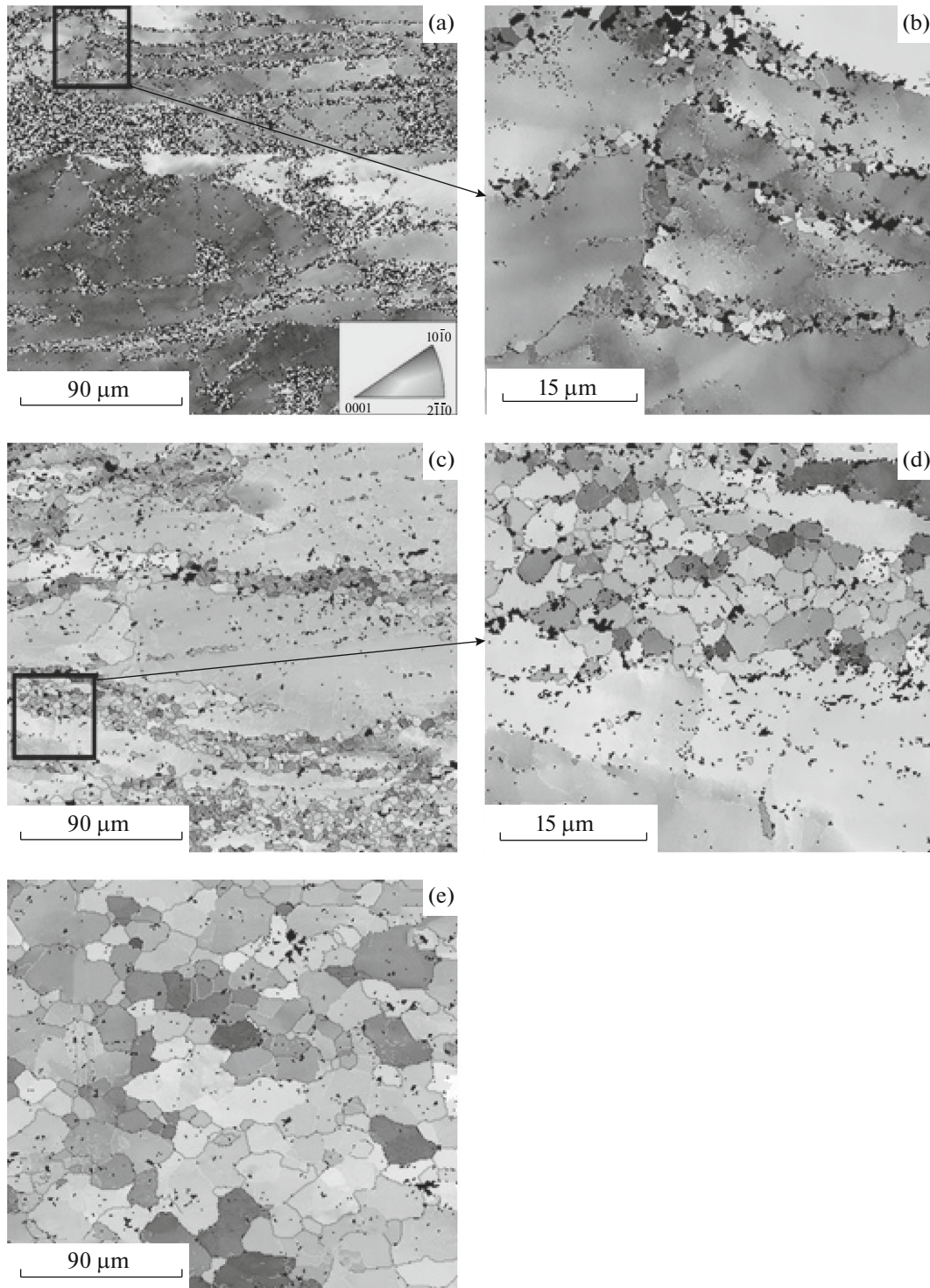


**Fig. 6.** Orientational maps of the Mg–0.8% Ca alloy in the initially homogenized state after 75% uniaxial compression at (a, b) 250, (c, d) 350, and (e) 450°C.

enized Mg–0.8% Ca alloy in the range 250–450°C. In addition to coarse primary particles, the a volume fraction of which is 1.2%, there are fairly uniformly distributed secondary fine equiaxed second-phase particles with an average size of  $\sim 0.3 \mu\text{m}$  and a volume

fraction of 2% in Mg–0.8% Ca alloy samples after uniaxial compression at 250°C (see Fig. 5b). An increase in the deformation temperature to 300°C weakly changes the distribution and the shape of the  $\text{Mg}_2\text{Ca}$  particles, but it changes their volume fraction,

which increases to ~2.5%. The volume fraction of coarse particles is 1.4% (Fig. 5b).

A similar picture is observed for compression temperatures of 350 and 400°C. The volume fractions of fine particles in these cases increase to 2.67 and 2.73%, respectively, but the total volume fraction of these particles in both cases is almost the same, ~5% (see Fig. 5b). Fine secondary-phase particles begin to precipitate from the solid solution after uniaxial compression at 450°C, which can indicate that the particles having precipitated from the solid solution in the upsetting temperature range 250–400°C are coherently related to the matrix.

However, the coherence is disrupted at the particle–matrix boundary upon uniaxial compression at 450°C, apparently, due to the intensive dynamic recrystallization-induced migration of grain boundaries. This explains the weakening the interaction between the matrix and the precipitated fine particles. The volume fraction of the fine particles in this case is highest, (3.07%), and the total volume fraction (including coarse particles) is 5.8% (Fig. 5b).

Figure 5b shows that both the volume fraction and the average particle size of the second phase as functions of the compression temperature have almost the same slope of the straight line. These parameters linearly increase with temperature in both cases. The average fine second-phase particle size increases from 0.3  $\mu\text{m}$  at 250°C to 0.48  $\mu\text{m}$  after upsetting at 450°C. The total volume fraction of the second phase changes from 3.3 to 5.8%.

The investigation of the mechanical properties and the regularities of the microstructure formation upon uniaxial compression of as-cast and homogenized Mg–0.8% Ca alloy samples showed that the behavior of the temperature dependences of the yield strength and flow stress of the samples is the same. Their strength properties decrease monotonically when the temperature is increased. The stage of steady flow appears on the stress–strain curves at 450°C for all states. The flow stress of the homogenized sample changes nonmonotonically with the strain in the temperature range 250–350°C as compared to that of the as-cast sample, in which it increases smoothly when strain is increased. The homogenized samples fail in a brittle manner at a deformation temperature of 250°C after a strain of ~30%, and the as-cast samples at the same temperature undergo deformation without fracture.

As the uniaxial compression temperature increases, the homogeneity of the structure increases in the samples in both states. EBSD analysis shows that plastic deformation during uniaxial compression of homogenized samples at 250°C is localized in narrow bands, whereas plastic deformation in the as-cast alloy samples is localized in relatively wide zones. According to EBSD analysis, an increase in the deformation temperature to 350°C widens the localized

deformation bands. A fine-grained recrystallized structure with a grain size of 2–6  $\mu\text{m}$  for the as-cast state and 0.8–3  $\mu\text{m}$  for the initially homogenized state is formed inside these deformation bands in the temperature range 250–350°C. A relatively homogeneous recrystallized structure with an average grain size of about 20  $\mu\text{m}$  is formed at  $t = 450^\circ\text{C}$ . According to OM, a small number of regions with recrystallized grains was observed only after deformation performed at 400°C. A relatively homogeneous recrystallized structure with an average grain size of 13 and 16.5  $\mu\text{m}$  was observed in both the as-cast and homogenized states, respectively, after deformation at 450°C.

Thus, the results of the compression tests suggested that multiaxial deformation should be carried out starting from a temperature of 450°C to obtain a mainly recrystallized structure.

#### *Effect of Multiaxial Deformation Conditions on the Microstructure and Mechanical Properties of the Mg–0.8% Ca Alloy*

The choice of multiaxial deformation conditions was based on the assumption that deformation should be started at 450°C to form a mainly recrystallized structure, and it then should be performed upon decreasing the deformation temperature to reach the minimum grain size. A stage-by-stage decrease in the deformation temperature can be used to achieve a smaller grain size at each subsequent stage in a recrystallized structure, which determines a lower critical strain at a subsequent stage to form a recrystallized structure [25]. The possibility to reach a smaller grain size by decreasing the temperature of multiaxial deformation was previously demonstrated by the example of the Mg–0.3% Ca alloy [22].

Figure 7a shows the average grain size (OM) as a function of the multiaxial deformation temperature of the initially homogenized Mg–0.8% Ca alloy. A relatively heterogeneous recrystallized structure was formed after the first pass of multiaxial deformation ( $t = 450^\circ\text{C}$ ). It included both grains of relatively small size and regions with rather coarse grains. The average grain size after the first pass of multiaxial deformation ( $t = 450^\circ\text{C}$ ) was 18.9  $\mu\text{m}$  (see Fig. 7a). The microstructure after the third (400°C), fifth (350°C), or seventh (300°C) pass undergoes insignificant changes as compared to the first pass: the structure also remains slightly heterogeneous, but the degree of heterogeneity decreases and the average grain size decreases to 11.5, 8, and 4  $\mu\text{m}$ , respectively (see Fig. 7a). The homogeneity of the structure of the Mg–0.8% Ca alloy reaches the highest level after nine passes of multiaxial deformation ( $t = 250^\circ\text{C}$ ). This structure has regular-shaped polyhedral grains with an average size of 2  $\mu\text{m}$  (Fig. 7a).

The structure of the homogenized Mg–0.8% Ca alloy after multiaxial deformation was also analyzed by

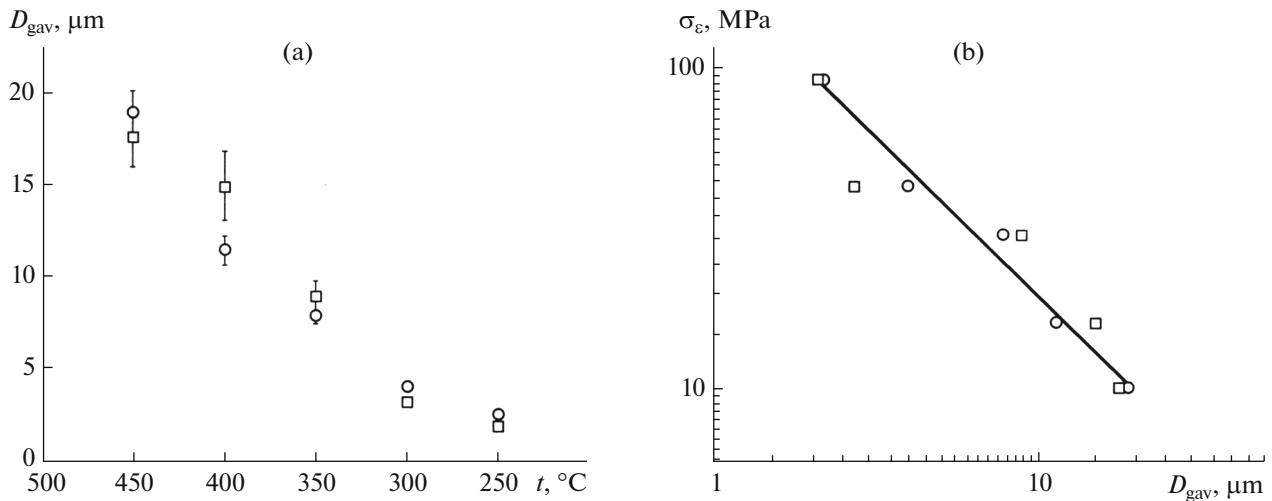


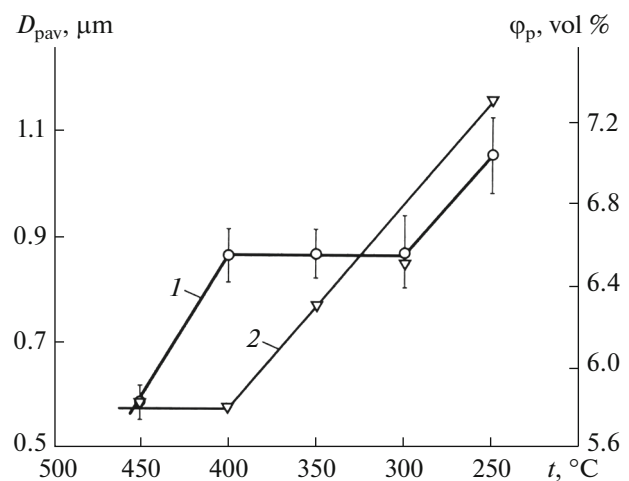
**Fig. 7.** (a) Average grain size  $D_{gav}$  vs. temperature  $t$ : ( $\square$ ) OM and ( $\circ$ ) EBSD. (b) Flow stress  $\sigma_{\epsilon}$  vs. the average grain size upon multiaxial deformation of the homogenized Mg–0.8% Ca.

EBSD. It can be seen that the average grain sizes determined by EBSD analysis is in agreement with that determined by OM (Fig. 7a). For example, the average grain size was about 17.7  $\mu\text{m}$  after the first pass of the multiaxial deformation, 8.9  $\mu\text{m}$  after the fifth, 3.4  $\mu\text{m}$  after the seventh, and 2.1  $\mu\text{m}$  after the ninth pass.

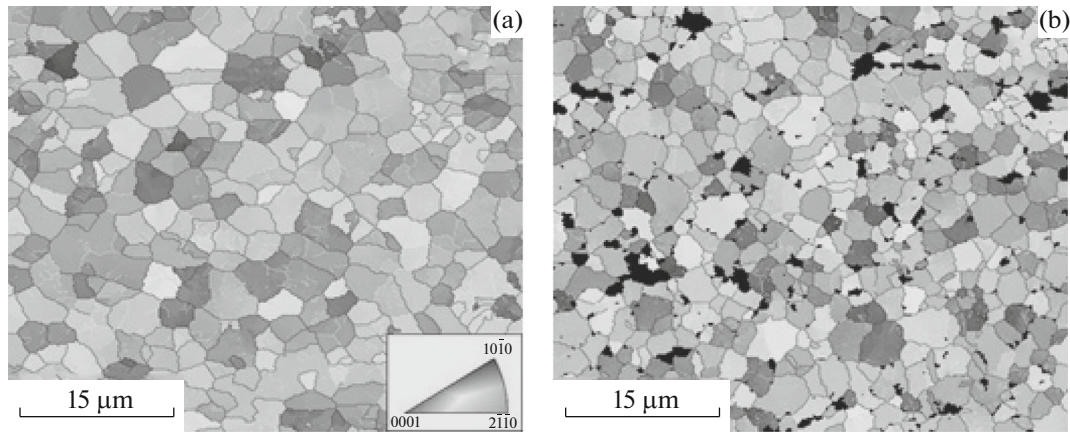
Figure 7b shows flow stress  $\sigma_{\epsilon}$  as a function of average grain size  $D_{gav}$  determined from OM and EBSD. All experimental points can be approximated by a linear dependence at a slope of the straight line of unity. The form of the curve suggests that structure formation is controlled by one process, the discontinuous dynamic recrystallization (DDR, the Bailey–Hirsch mechanism), in the entire temperature range. It is worth noting that DDR usually is observed in magnesium alloys at high temperatures, such as 450  $^{\circ}\text{C}$ . A controlling mechanism at low temperatures (250  $^{\circ}\text{C}$ ) is usually continuous dynamic recrystallization (the Cahn–Burgers mechanism) [26].

Figure 8 shows the average particle size and the volume fraction of second-phase as functions of the temperature of the multiaxial compression of the homogenized Mg–0.8% Ca alloy. There are two kinds of particles in the structure after the first pass of multiaxial deformation ( $t = 450^{\circ}\text{C}$ ): relatively fine ( $D_{pav} \approx 0.58 \mu\text{m}$ ) particles, which are mainly equiaxed in shape, and coarse particles, which are mainly irregular in shape ( $D_{pav} \approx 3.6 \mu\text{m}$ ). The total volume fraction of two kinds of particles after the first deformation cycle is 5.8% (see Fig. 8). The size of the fine Mg<sub>2</sub>Ca particles after three multiaxial deformation passes ( $t = 400^{\circ}\text{C}$ ) increases to 0.87  $\mu\text{m}$ , but their volume fraction remains the same, 5.8% (Fig. 8). An increase in the number of passes to seven ( $t = 300^{\circ}\text{C}$ ) does not cause any significant changes in the distribution of these

particles and in their morphology. The average size of fine particles in the temperature range 400–300  $^{\circ}\text{C}$  varies within the measurement error and is 0.9  $\mu\text{m}$ , whereas the total volume fraction of the Mg<sub>2</sub>Ca particles after seven passes ( $t = 300^{\circ}\text{C}$ ) increases by 0.7% (to 6.5%). Nine passes of the multiaxial deformation ( $t = 250^{\circ}\text{C}$ ) increase both the average particle size and the volume fraction of the second phase. In particular, the particle size increases to  $\sim 1 \mu\text{m}$ , and the total volume fraction of the particles increases from 6.5 to 7.3% (Fig. 8). It is interesting that the similar evolution of the average size can be observed in the case of coarse particles. The average size of coarse particles before seven multiaxial deformation passes ( $t = 300^{\circ}\text{C}$ ) varies only slightly and is  $\sim 3.7 \mu\text{m}$ , that is within the error of



**Fig. 8.** (1) Average particle size  $D_{pav}$  and (2) volume fraction of second-phase  $\phi_p$  as functions of the temperature of the multiaxial compression of the homogenized Mg–0.8% Ca alloy.



**Fig. 9.** Orientational maps of both (a) as-cast and (b) homogenized Mg–0.8% Ca alloy samples after nine passes of multi-axial deformation.

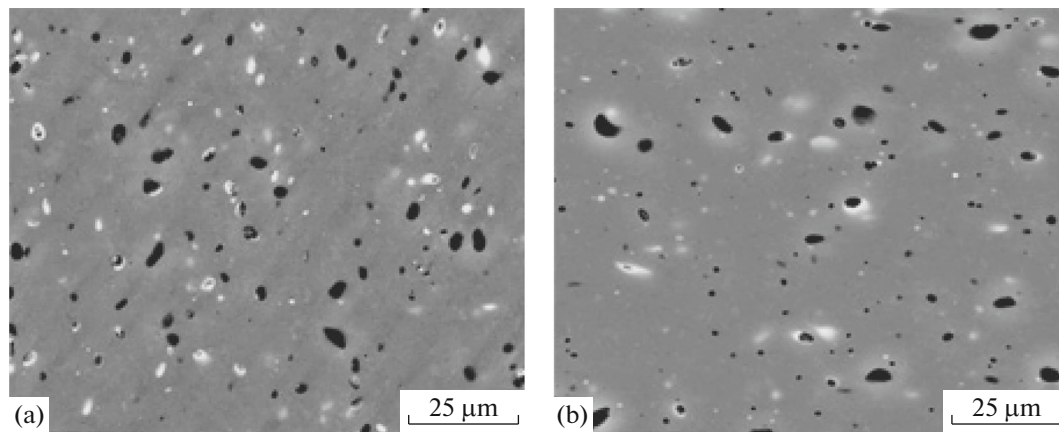


**Fig. 10.** SEM images of the second-phase particles in both (a) as-cast and (b) homogenized Mg–0.8% Ca alloy samples after nine passes of multi-axial deformation.

measurement. It reaches maximum after nine passes (250°C) and is  $\sim 4.7 \mu\text{m}$ , whereas the size of individual particles is  $\sim 10 \mu\text{m}$ . This coarsening of particles is often accompanied by a change in their shape.

Figure 9 displays the orientational maps after nine passes of the multi-axial compression of the as-cast and homogenized samples. Figures 9a and 9b suggest that the degree of structure uniformity of the homogenized sample is higher than that of the as-cast sample. In particular, recrystallized grains whose average size is  $2.1 \mu\text{m}$  have a regular polyhedral shape practically in the entire volume of the first sample; the fraction of HAB is 68.2%. However, there are regions in which dynamic recrystallization has not been fully completed in the as-cast sample after deformation. This assumption is supported by the presence of a number of regions with coarse grains, with bent boundaries, and surrounded by chains of fine equiaxed grains (Fig. 9a). The average grain size in this case is  $2.8 \mu\text{m}$  and the fraction of HAB is 57.6%.

Comparison of second-phase particles in both (a) as-cast and (b) homogenized Mg–0.8% Ca alloy samples after nine passes of multi-axial deformation (Figs. 10a, 10b) showed the following. The  $\text{Mg}_2\text{Ca}$  particles in the as-cast sample after nine passes (see Fig. 10a) often acquire an elongated shape as compared to those in the homogenized sample after similar deformation that are predominantly equiaxed-shaped. The average particle size in the initial as-cast sample is  $1.6 \mu\text{m}$  and their volume fraction is 6.1%. The average size of the equiaxed particles in the homogenized sample after nine passes is  $\sim 1 \mu\text{m}$ , and their volume fraction is slightly higher than that in the as-cast sample after deformation and is 6.5%.

Figure 11 depicts stress–strain curves for the Mg–0.8% Ca alloy after uniaxial tension. Table 2 shows yield strength  $\sigma_{0.2}$ , tensile strength  $\sigma_u$ , and relative elongation  $\delta$  determined from mechanical tests. The as-cast alloy exhibits the low strength: a yield strength of 51 and a tensile strength of 97 MPa. The plasticity in

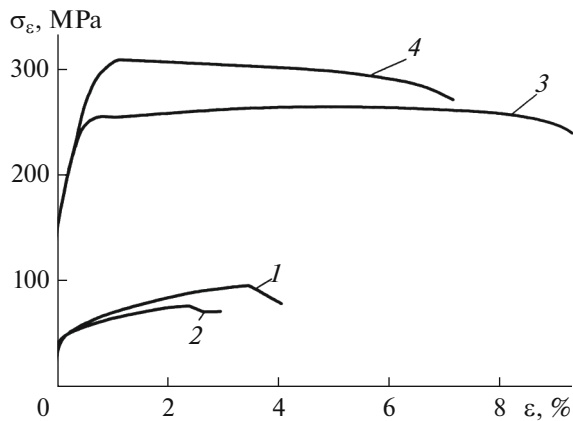


**Fig. 11.** Flow stress  $\sigma_{\varepsilon}$  vs. strain  $\varepsilon$  determined during the uniaxial tension of the Mg–0.8% Ca alloy samples in the (1) as-cast and (2) homogenized states and after multi-axial deformation of (3) as-cast and (4) homogenized samples.

this state is also low and the relative elongation is only 4.1%. Homogenization significantly deteriorates the mechanical properties: tensile strength  $\sigma_u$  and relative elongation  $\delta$  decrease to 78 MPa and 3%, respectively. However, the yield strength remains unchanged (about 50 MPa). The strength after multi-axial deformation of the samples in both states significantly increases. The yield strength of both as-cast and homogenized samples increases by a factor of about 4 (to 199 and 193, respectively). At similar  $\sigma_{0.2}$ , a homogenized sample has a tensile strength of 308 MPa, whereas  $\sigma_u$  of the as-cast sample after deformation is somewhat lower (264 MPa). However, the plasticity of the alloy in the cast state is higher ( $\delta = 9.4\%$ ) than in the homogenized state ( $\delta = 7.2\%$ ).

The greater increase in the ultimate tensile strength after multi-axial deformation of the homogenized Mg–0.8% Ca alloy can be explained by a slightly smaller grain size, a slightly smaller  $Mg_2Ca$  particle size, and a slightly larger volume fraction of these particles. An increase in the plasticity after multi-axial deformation seems to be associated with scattering of the sharp

prismatic texture, as it was observed in the case of an Mg–0.3% Ca alloy [21].

When the deformation temperature is decreased, multi-axial deformation was found to enhance the mechanical properties of the Mg–0.8% Ca alloy significantly.

## CONCLUSIONS

(1) Structure examination showed that the structure homogeneity in both as-cast and homogenized Mg–0.8% Ca alloys during uniaxial compression increases with temperature. Plastic deformation localizes in narrow deformation bands in the homogenized sample upon deformation at 250°C, and it localizes in relatively wide zones in the as-cast sample. Deformation at 350°C widens localized deformation bands. A fine-grained recrystallized structure is formed inside these bands. A relatively homogeneous recrystallized structure with an average grain size of about 20  $\mu\text{m}$  is formed in both states after uniaxial compression at  $t = 450^\circ\text{C}$ .

(2) Multi-axial deformation significantly refines the initial coarse-grained structure of the Mg–0.8% Ca alloy, when the temperature is decreased. A homogeneous recrystallized structure with an average grain size of 2.1  $\mu\text{m}$  and a HAB fraction of 68.2% forms after nine passes of multi-axial compression (last at  $t = 250^\circ\text{C}$ ) of the homogenized samples.

(3) It was found that the structure-forming mechanism in the entire temperature range of the multi-axial deformation of the Mg–0.8% Ca alloy is discontinuous dynamic recrystallization.

(4) Microstructure refinement causes a significant increase in the mechanical properties of the Mg–0.8% Ca alloy. The yield strength of the deformed samples increases by a factor of about 4 (to 199 and 193, respectively), as compared to the initial as-cast and homogenized states. The tensile strength of the homogenized sample after multi-axial deformation is 308 MPa, and that of the as-cast sample is 264 MPa. The relative elongation of the Mg–0.8% Ca alloy after multi-axial deformation of both initial states increases by more than two times.

**Table 2.** Yield strength, tensile strength, and relative elongation of the Mg–0.8% Ca alloy in different states

State	$\sigma_{0.2}$	$\sigma_u$	$\delta, \%$
	MPa		
Cast sample:			
initial	51	97	4.1
after multi-axial deformation	199	264	9.4
Homogenized sample:			
initial	50	78	3.0
after multi-axial deformation	193	308	7.2

## ACKNOWLEDGMENTS

This work was supported by the Russian Scientific Foundation, project no. 17-13-01488.

## REFERENCES

1. L. Mordike and T. Ebert, "Magnesium: properties—applications—potential," *Mater. Sci. Eng. A*, **302**, 37–45 (2001).
2. E. F. Volkova, "Present-day deformable magnesium alloys and composite materials," *Metalloved. Term. Obrab. Met.*, No. 11, 5–9 (2006).

3. E. F. Volkova and I. Yu. Mukhina, "New magnesium materials and highly resourceful technologies for their production," *Tekhnol. Legk. Splavov*, No. 2, 28–34 (2007).
4. S. Virtanen, "Biodegradable Mg and Mg alloys: corrosion and biocompatibility," *Mater. Sci. Eng. B* **176**, 1600–1608 (2011).
5. S. Agarwal, J. Curtin, B. Duffy, et al., "Biodegradable magnesium alloys for orthopedic applications: a review on corrosion, biocompatibility and surface modifications," *Mater. Sci. Eng. C* **68**, 948–963 (2016).
6. R. Waksman, "Biodegradable stents: they do their job and disappear," *Invasive Cardiol.* **18** (2), 70–74 (2006).
7. L. Tan, X. Yu, P. Wan, et al., "Biodegradable materials for bone repairs: a review," *Mater. Sci. Technol.* **29** (6), 603–513 (2013).
8. F. Witte, Y. F. Zheng, and X. N. Gu, "Biodegradable metals," *Mater. Sci. Eng. R* **77**, 1–34 (2014).
9. Y. Chen, Z. Xu, C. Smith, and J. Sankar, "Recent advances on the development of magnesium alloys for biodegradable implants: review," *Acta Biomater.* **10**, 4561–4573 (2014).
10. Y. Liu, S. Zheng, N. Li, H. Guo, et al., "Study on the in vitro degradation behavior of pure Mg and WE43 in human bile for 60 days for future usage in biliary," *Mater. Lett.* **179**, 100–103 (2016).
11. G. E. Poinern, S. Brundavanam, and D. Fawcett "Bio-medical magnesium alloys: a review of material properties, surface modifications and potential as a biodegradable orthopaedic implant," *Amer. J. Biomed. Eng.* **2**, 218–240 (2012).
12. L. Xu, F. Pan, G. Yu, et al., "In vitro and in vivo evaluation of the surface bioactivity of a calcium phosphate coated magnesium alloy," *Biomaterials* **30** 1512–1523 (2009).
13. S. V. Dobatkin, E. A. Lukyanova, N. S. Martynenko, et al., "Strength, corrosion resistance, and biocompatibility of ultrafine-grained Mg alloys after different modes of severe plastic deformation," *Mater. Sci. Eng.* **194** 012004 (2017). doi 10.1088/1757-899X/194/1/012004
14. R. Z. Valiev, A. P. Zhilyaev, and T. J. Langdon, *Volume Nanostructured Materials: Fundamentals and Applications* (Eko Vektor, St. Petersburg, 2017).
15. S. R. Agnew, P. Mehrotra, T. M. Lillo, G. M. Stoica, and P. K. Liaw, "Texture evolution of five wrought magnesium alloys during route A equal channel angular extrusion: experiments and simulations," *Acta Mater.* **53**, 3135–3146 (2005).
16. P. Minárik, J. Veselý, R. Kráí, and J. Bohlen, "Exceptional mechanical properties of ultrafine grain Mg–4Y–3Re alloy processed by ECAP," *Mater. Sci. Eng. A* **708**, 193–198 (2017).
17. V. N. Serebryany, G. S. D'yakonov, V. I. Kopylov, G. A. Salishchev, and S. V. Dobatkin, "Texture and structure contribution to low-temperature plasticity enhancement of Mg–Al–Zn–Mn Alloy MA21pch after ECAP and annealing," *Phys. Met. Metallogr.* **115** (5), 448–456 (2013).
18. V. N. Serebryanyi, V. Yu. Perezhogin, G. I. Raab, V. I. Kopylov, N. Yu. Tabachkova, V. P. Sirotinkin, and S. V. Dobatkin, "Structure, texture, and mechanical properties of an MA2-1pch magnesium alloy after two-stage equal-channel angular pressing and intermediate annealing," *Russ. Metall. (Metally)*, No. 1, 36–42 (2015).
19. N. S. Martynenko, E. A. Lukyanova, V. N. Serebryany, et al., "Increasing strength and ductility of magnesium alloy WB43 by equal-channel angular pressing," *Mater. Sci. Eng. A* **712**, 625–629 (2018).
20. J. Xing, H. Soda, X. Yang, et al. "Ultra-fine grain development in an AZ31 magnesium alloy during multi-directional forging under decreasing temperature conditions," *Mater. Trans.* **46** (7), 1646–1650 (2005).
21. K. Funami and M. Noda, "Grain refinement of magnesium alloy by multiaxial alternative forging and hydrogenation treatment," *Magnesium Alloys: Des., Process. Prop.*, 245–264 (2011). doi 10.5772/13189
22. S. V. Dobatkin, L. L. Rokhlin, G. A. Salishchev, et al., "Structure and properties of an Mg–0.3% Ca magnesium alloy after multiaxial deformation and equal-channel angular pressing," *Russ. Metall. (Metally)*, No. 11, 911–919 (2014).
23. S. V. Dobatkin, G. A. Salishchev, A. A. Kuznetsov, et al., "Comparative analysis of the structure and properties of oxygen-free copper after different severe plastic deformation techniques," *Fiz. Tekh. Vys. Davlenii* **16** (4), 23–36 (2006).
24. S. V. Dobatkin, G. A. Salishchev, A. A. Kuznetsov, and T. N. Kon'kova, "Submicrocrystalline structure in copper after different severe plastic deformation schemes," *Mater. Sci. Forum.* **558–559**, 189–194 (2007).
25. S. S. Gorelik, S. V. Dobatkin, and L. M. Kaputkina, *Recrystallization of Metals and Alloys* (MISiS, Moscow, 2005).
26. A. Galiev, R. Kaibyshev, and G. Gottstein, "Correlation of plastic deformation and dynamic recrystallization in magnesium alloy ZK60," *Acta Mater.* **49**, 1199–1207 (2001).

*Translated by T. Gapontseva*